

Electromagnetic form factors of the baryon octet in the perturbative chiral quark model

S. Cheedket^{1,2}, V. E. Lyubovitskij¹ Th. Gutsche¹, Amand Faessler¹,
K. Pumsa-ard¹, and Y. Yan²

¹ Institut für Theoretische Physik, Universität Tübingen, Auf der Morgenstelle 14, D-72076 Tübingen, Germany

² School of Physics, Institute of Science, Suranaree University of Technology, Nakhon Ratchasima 30000, Thailand

Received: date / Revised version: date

Abstract. We apply the perturbative chiral quark model at one loop to analyze the electromagnetic form factors of the baryon octet. The analytic expressions for baryon form factors, which are given in terms of fundamental parameters of low-energy pion-nucleon physics (weak pion decay constant, axial nucleon coupling, strong pion-nucleon form factor), and the numerical results for baryon magnetic moments, charge and magnetic radii are presented. Our results are in good agreement with experimental data.

PACS. 12.39.Ki Relativistic quark model – 13.40.Em Electric and magnetic moments – 13.40.Gp Electromagnetic form factors – 14.20.Dh Protons and neutrons – 14.20.Jn Hyperons

1 Introduction

The study of the electromagnetic form factors of baryons is a very important first step in understanding their internal structure. At present, electromagnetic form factors and related properties (magnetic moments, charge and magnetic radii) of the nucleon have been measured precisely, but for the hyperons data rarely exist with the exception of the magnetic moments. Recently, the charge radius of the Σ^- has been measured [1,2] and therefore gives a first estimate of the charge form factor of the hyperon at low momentum transfers.

In Refs. [3]–[8] we developed the perturbative chiral quark model (PCQM) for the study of baryon properties: electromagnetic form factors of the nucleon, low-energy meson-baryon scattering and σ -terms, electromagnetic excitation of nucleon resonances, etc. In Ref. [3] the PCQM has been applied to study the electromagnetic form factors of the nucleon and the results obtained are in good agreement with experimental data. In this paper we extend the PCQM to study the electromagnetic form factors of hyperons and give predictions with respect to future measurements of their magnetic moments, radii and the momentum dependence of form factors. We proceed as follows. In Sect. 2 we describe the basic notions of our approach. In Sect. 3 we present the analytic expressions for the charge and magnetic form factors of the baryon octet. Numerical results for their magnetic moments, charge and magnetic radii, and the momentum dependence of the form factors are discussed in Sect. 4. Sect. 5 contains a summary.

2 The Perturbative Chiral Quark Model

2.1 Effective Lagrangian and zeroth order properties

The following considerations are based on the perturbative chiral quark model (PCQM) [3,4]. The PCQM is a relativistic quark model which is based on an effective Lagrangian $\mathcal{L}_{\text{eff}} = \mathcal{L}_{\text{inv}}^{\text{lin}} + \mathcal{L}_{\chi SB}$. The Lagrangian includes the linearized chiral invariant term $\mathcal{L}_{\text{inv}}^{\text{lin}}$ and a mass term $\mathcal{L}_{\chi SB}$ which explicitly breaks chiral symmetry

$$\mathcal{L}_{\text{inv}}^{\text{lin}} = \bar{\psi}(x) [i\partial - \gamma^0 V(r) - S(r)] \psi(x) + \frac{1}{2} \sum_{i=1}^8 [\partial_\mu \Phi_i(x)]^2 - \bar{\psi}(x) S(r) i\gamma^5 \frac{\hat{\Phi}(x)}{F} \psi(x), \quad (1)$$

$$\mathcal{L}_{\chi SB} = -\bar{\psi}(x) \mathcal{M} \psi(x) - \frac{B}{2} \text{Tr}[\hat{\Phi}^2(x) \mathcal{M}], \quad (2)$$

where $r = |\mathbf{x}|$; ψ is the quark field; $\hat{\Phi}$ is the matrix of the pseudoscalar mesons; $S(r)$ and $V(r)$ are scalar and vector components of an effective, static potential providing quark confinement; $\mathcal{M} = \text{diag}\{\hat{m}, \hat{m}, m_s\}$ is the mass matrix of current quarks (we restrict to the isospin symmetry limit with $m_u = m_d = \hat{m}$); B is the quark condensate parameter; and $F = 88$ MeV is the pion decay constant in the chiral limit. We rely on the standard picture of chiral symmetry breaking and for the masses of pseudoscalar mesons we use the leading term in chiral expansion (i.e. linear in the current quark mass): $M_\pi^2 = 2\hat{m}B$, $M_K^2 = (\hat{m} + m_s)B$, $M_\eta^2 = \frac{2}{3}(\hat{m} + 2m_s)B$. Meson masses satisfy the Gell-Mann–Oakes–Renner and the Gell-Mann–Okubo relation $3M_\eta^2 + M_\pi^2 = 4M_K^2$. In the evaluation we

use the following set of QCD parameters: $\hat{m} = 7$ MeV, $m_s/\hat{m} = 25$ and $B = M_{\pi^+}^2/(2\hat{m}) = 1.4$ GeV.

To describe the properties of baryons which are modelled as bound states of valence quarks surrounded by a meson cloud we formulate perturbation theory. In our approach the mass (energy) m_N^{core} of the three-quark core of the nucleon is related to the single quark energy \mathcal{E}_0 by $m_N^{\text{core}} = 3\mathcal{E}_0$. For the unperturbed three-quark state we introduce the notation $|\phi_0\rangle$ with the appropriate normalization $\langle\phi_0|\phi_0\rangle = 1$. The single quark ground state energy \mathcal{E}_0 and wave function (WF), $u_0(\mathbf{x})$ are obtained from the Dirac equation

$$[-i\boldsymbol{\alpha} \cdot \boldsymbol{\nabla} + \beta S(r) + V(r) - \mathcal{E}_0] u_0(\mathbf{x}) = 0. \quad (3)$$

The quark WF $u_0(\mathbf{x})$ belongs to the basis of potential eigenstates (including excited quark and antiquark solutions) used for expansion of the quark field operator $\psi(x)$. Here we restrict the expansion to the ground state contribution with $\psi(x) = b_0 u_0(\mathbf{x}) \exp(-i\mathcal{E}_0 t)$, where b_0 is the corresponding single quark annihilation operator. In Eq. (3) the current quark mass is not included to simplify our calculational technique. Instead, we consider the quark mass term as a small perturbation.

For a given form of the potentials $S(r)$ and $V(r)$ the Dirac equation in Eq. (3) can be solved numerically. Here, for the sake of simplicity, we use a variational Gaussian ansatz for the quark wave function given by the analytical form:

$$u_0(\mathbf{x}) = N \exp\left[-\frac{\mathbf{x}^2}{2R^2}\right] \left(i\rho \frac{\boldsymbol{\sigma} \cdot \mathbf{x}}{R}\right) \chi_s \chi_f \chi_c, \quad (4)$$

where $N = [\pi^{3/2} R^3 (1 + 3\rho^2/2)]^{-1/2}$ is a constant fixed by the normalization condition $\int d^3x u_0^\dagger(\mathbf{x}) u_0(\mathbf{x}) \equiv 1$; χ_s , χ_f , χ_c are the spin, flavor and color quark wave functions, respectively. Our Gaussian ansatz contains two model parameters: the dimensional parameter R and the dimensionless parameter ρ . The parameter ρ can be related to the axial coupling constant g_A calculated in zeroth-order (or 3q-core) approximation:

$$g_A = \frac{5}{3} \left(1 - \frac{2\rho^2}{1 + \frac{3}{2}\rho^2}\right) = \frac{5}{3} \frac{1 + 2\gamma}{3}, \quad (5)$$

where $\gamma = 9g_A/10 - 1/2$. The parameter R can be physically understood as the mean radius of the three-quark core and is related to the charge radius $\langle r_E^2 \rangle_{LO}^p$ of the proton in the leading-order (LO) approximation as

$$\langle r_E^2 \rangle_{LO}^p = \frac{3R^2}{2} \frac{1 + \frac{5}{2}\rho^2}{1 + \frac{3}{2}\rho^2} = R^2 \left(2 - \frac{\gamma}{2}\right). \quad (6)$$

In our calculations we use the value $g_A = 1.25$. We therefore have only one free parameter, that is R . In the final numerical evaluation R is varied in the region from 0.55 fm to 0.65 fm, which is sufficiently large to justify perturbation theory.

In the PCQM confinement is introduced as a static mean field potential, hence covariance cannot be fulfilled.

As a consequence matrix elements are frame dependent: both Galilei invariance of the zeroth order baryon wave functions and Lorentz boost effects, when considering finite momenta transfers, are neglected. Approximate techniques [9,10] have been developed to account for these deficiencies in static potential models. However, these techniques do not always agree and lead to further ambiguities in model evaluations. Furthermore, existing Galilean projection techniques are known to lead to conflicts with chiral symmetry constraints [4]. In the present manuscript we completely neglect the study of these additional model dependent effects. We focus on the role of meson loops, which, as was shown in the context of the cloudy bag model [10], are not plagued by these additional uncertainties.

2.2 Renormalization of the PCQM and perturbation theory

We consider perturbation theory up to one meson loop and up to terms linear in the current quark mass. The formalism utilizes a renormalization technique, which, by introduction of counterterms, effectively reduces the number of Feynman diagrams to be evaluated. For details of this technique we refer to the Ref. [3]. Here we briefly describe the basic ingredients relevant for the further discussion. We define the renormalized current quark masses, \hat{m}^r and m_s^r and the renormalization constants, \hat{Z} and Z_s as :

$$\hat{m}^r = \hat{m} - \frac{3}{400\gamma} \left(\frac{g_A}{\pi F}\right)^2 \int_0^\infty dp p^4 F_{\pi NN}(p^2) \times \left\{ \frac{9}{w_\pi^2(p^2)} + \frac{6}{w_K^2(p^2)} + \frac{1}{w_\eta^2(p^2)} \right\}, \quad (7)$$

$$m_s^r = m_s - \frac{3}{400\gamma} \left(\frac{g_A}{\pi F}\right)^2 \int_0^\infty dp p^4 F_{\pi NN}(p^2) \times \left\{ \frac{12}{w_K^2(p^2)} + \frac{4}{w_\eta^2(p^2)} \right\}, \quad (8)$$

$$\hat{Z} = 1 - \frac{3}{400} \left(\frac{g_A}{\pi F}\right)^2 \int_0^\infty dp p^4 F_{\pi NN}(p^2) \times \left\{ \frac{9}{w_\pi^3(p^2)} + \frac{6}{w_K^3(p^2)} + \frac{1}{w_\eta^3(p^2)} \right\}, \quad (9)$$

$$Z_s = 1 - \frac{3}{400} \left(\frac{g_A}{\pi F}\right)^2 \int_0^\infty dp p^4 F_{\pi NN}(p^2) \times \left\{ \frac{12}{w_K^3(p^2)} + \frac{4}{w_\eta^3(p^2)} \right\}. \quad (10)$$

For a meson with three-momentum \mathbf{p} the meson energy is $w_\phi(p^2) = \sqrt{M_\phi^2 + p^2}$ with $p = |\mathbf{p}|$ and $F_{\pi NN}(p^2)$ is the πNN form factor normalized to unity at zero recoil ($\mathbf{p} = 0$) :

$$F_{\pi NN}(p^2) = \exp\left(-\frac{p^2 R^2}{4}\right) \left\{ 1 + \frac{p^2 R^2}{8} \left(1 - \frac{5}{3g_A}\right) \right\}. \quad (11)$$

By adding the renormalized current quark mass term to the Dirac equation of Eq. (3) we obtain the renormalized

quark field ψ^r as :

$$\psi_i^r(x; m_i^r) = b_0 u_0^r(\mathbf{x}; m_i^r) \exp[-i\mathcal{E}_0^r(m_i^r)t], \quad (12)$$

where i is the flavor SU(3) index. The renormalized single quark WF $u_0^r(\mathbf{x}; m_i^r)$ and energy $\mathcal{E}_0^r(m_i^r)$ are related to the bare expressions $u_0(\mathbf{x})$ and \mathcal{E}_0 as :

$$u_0^r(\mathbf{x}; m_i^r) = u_0(\mathbf{x}) + \delta u_0(\mathbf{x}; m_i^r), \quad (13)$$

$$\mathcal{E}_0^r(m_i^r) = \mathcal{E}_0 + \delta\mathcal{E}_0^r(m_i^r), \quad (14)$$

where

$$\begin{aligned} \delta u_0(\mathbf{x}; m_i^r) &= \frac{m_i^r}{2} \frac{\rho R}{1 + \frac{3}{2}\rho^2} \\ &\times \left(\frac{\frac{1}{2} + \frac{21}{4}\rho^2}{1 + \frac{3}{2}\rho^2} - \frac{\mathbf{x}^2}{R^2} + \gamma^0 \right) u_0(\mathbf{x}), \end{aligned} \quad (15)$$

$$\delta\mathcal{E}_0^r(m_i^r) = \gamma m_i^r. \quad (16)$$

Introduction of the electromagnetic field A_μ is accomplished by adding the kinetic energy term and by standard minimal substitution in the Lagrangian of Eq. (1) and Eq. (2) with

$$\partial_\mu \psi^r \longrightarrow D_\mu \psi^r = \partial_\mu \psi^r + ieQ A_\mu \psi^r, \quad (17)$$

$$\partial_\mu \Phi_i \longrightarrow D_\mu \Phi_i = \partial_\mu \Phi_i + e \left[f_{3ij} + \frac{f_{8ij}}{\sqrt{3}} \right] A_\mu \Phi_j, \quad (18)$$

where Q is the quark charge matrix and f_{ijk} are the totally antisymmetric structure constants of SU(3). The renormalized effective Lagrangian is obtained from the original one of Eqs. (1) and (2) by replacing ψ with ψ^r , adding the counterterms and by standard minimal substitution. From this we derive the electromagnetic renormalized current operator as :

$$j_r^\mu = j_{\psi^r}^\mu + j_\Phi^\mu + \delta j_{\psi^r}^\mu. \quad (19)$$

It contains the quark component $j_{\psi^r}^\mu$, the charged meson component j_Φ^μ , and the contribution of the counterterm $\delta j_{\psi^r}^\mu$:

$$\begin{aligned} j_{\psi^r}^\mu &= \bar{\psi}^r \gamma^\mu Q \psi^r \\ &= \frac{1}{3} [2\bar{u}^r \gamma^\mu u^r - \bar{d}^r \gamma^\mu d^r - \bar{s}^r \gamma^\mu s^r], \end{aligned} \quad (20)$$

$$\begin{aligned} j_\Phi^\mu &= \left[f_{3ij} + \frac{f_{8ij}}{\sqrt{3}} \right] \Phi_i \partial^\mu \Phi_j \\ &= [\pi^- i \partial^\mu \pi^+ - \pi^+ i \partial^\mu \pi^- \\ &\quad + K^- i \partial^\mu K^+ - K^+ i \partial^\mu K^-], \end{aligned} \quad (21)$$

$$\begin{aligned} \delta j_{\psi^r}^\mu &= \bar{\psi}^r (Z - 1) \gamma^\mu Q \psi^r \\ &= \frac{1}{3} [2\bar{u}^r (\hat{Z} - 1) \gamma^\mu u^r - \bar{d}^r (\hat{Z} - 1) \gamma^\mu d^r \\ &\quad - \bar{s}^r (Z_s - 1) \gamma^\mu s^r]. \end{aligned} \quad (22)$$

Following the Gell-Mann and Low theorem we define the expectation value of an operator \hat{O} for the renormalized PCQM by

$$\begin{aligned} \langle \hat{O} \rangle &= {}^B \langle \phi_0 | \sum_{n=0}^{\infty} \frac{i^n}{n!} \int i\delta(t_1) d^4 x_1 \dots d^4 x_n \\ &\quad \times T[\mathcal{L}_r^{str}(x_1) \dots \mathcal{L}_r^{str}(x_n) \hat{O}] | \phi_0 \rangle >^B. \end{aligned} \quad (23)$$

In Eq. (23) the superscript B indicates that the matrix elements are projected on the respective baryon states, the subscript c refers to contributions from connected graphs only and the renormalized strong interaction Lagrangian \mathcal{L}_r^{str} , which is treated as a perturbation, is defined as

$$\mathcal{L}_r^{str} = \mathcal{L}_I^{str} + \delta\mathcal{L}^{str}, \quad (24)$$

where

$$\mathcal{L}_I^{str} = -\bar{\psi}^r(x) i\gamma^5 \frac{\hat{\Phi}(x)}{F} S(r) \psi^r(x). \quad (25)$$

$\delta\mathcal{L}^{str}$ is the strong interaction part of the counterterms (see details in Ref. [3]). We evaluate Eq. (23) at one loop to the order $o(1/F^2)$ using Wick's theorem and the appropriate propagators. For the quark field we use a Feynman propagator for a fermion in a binding potential with

$$\begin{aligned} iG_\psi(x, y) &= \langle 0 | T \{ \psi(x) \bar{\psi}(y) \} | 0 \rangle \\ &= \theta(x_0 - y_0) \sum_{\alpha} u_{\alpha}(\mathbf{x}) \bar{u}_{\alpha}(\mathbf{y}) e^{-i\mathcal{E}_{\alpha}(x_0 - y_0)} \\ &\quad - \theta(y_0 - x_0) \sum_{\beta} v_{\beta}(\mathbf{x}) \bar{v}_{\beta}(\mathbf{y}) e^{i\mathcal{E}_{\beta}(x_0 - y_0)}. \end{aligned} \quad (26)$$

Up to order of accuracy we are working in it is sufficient to use $G_\psi(x, y)$ instead of $G_{\psi^r}(x, y)$ where renormalized quark fields are used. By restricting the summation over intermediate quark states to the ground state we get

$$\begin{aligned} iG_\psi(x, y) &\rightarrow iG_\psi^{(0)}(x, y) \\ &= u_0(\mathbf{x}) \bar{u}_0(\mathbf{y}) e^{-i\mathcal{E}_0(x_0 - y_0)} \theta(x_0 - y_0). \end{aligned} \quad (27)$$

Such a truncation can be considered as an additional regularization of the quark propagator, where in the case of SU(2)-flavor intermediate baryon states in loop-diagrams are restricted to N and Δ . From our previous works [3]-[8] we conclude that the use of a truncated quark propagator leads to a reasonable description of experimental data. In Ref. [8] we included, for the first time, excited quark states in the propagator of Eq. (26) and analyzed their influence on the matrix elements for the N - Δ transitions considered. We included the following set of excited quark states: the first p -states ($1p_{1/2}$ and $1p_{3/2}$ in the non-relativistic notation) and the second excited states ($1d_{3/2}$, $1d_{5/2}$ and $2s_{1/2}$). Again, we solved the Dirac equation analytically for the same form of the effective potential $V_{\text{eff}}(r) = S(r) + \gamma^0 V(r)$ as was done for the ground state. The corresponding expressions for the wave functions of the excited quark states are given in the Appendix.

In Ref. [8] we demonstrated that the excited quark states can increase the contribution of the loop diagrams but in comparison to the leading order (three-quark core) diagram this effect was of the order of 10%. In the context of the electromagnetic properties of baryons, we also estimated the effect of excited states, which again is of the order of 10%. However, there are quantities (like, e.g., the charge radius of neutron) which are dominated by higher-order effects. Particularly, in the $SU(2)$ flavor limit there is no three-quark core diagram contributing to this quantity. Only meson-loop diagram contribute to the neutron charge radius in the context of the PCQM and, therefore, the effects of excited states can be essential. In this paper (see Sec.4) we discuss the effects of excited states only for the neutron charge radius. We found that these effects considerably improved our prediction for the neutron charge radius close to the experimental result.

For the meson fields we use the free Feymann propagator for a boson with

$$\begin{aligned} i\Delta_{ij}(x-y) &= \langle 0|T\{\Phi_i(x)\Phi_j(y)\}|0\rangle \\ &= \delta_{ij} \int \frac{d^4k}{(2\pi)^4 i} \frac{\exp[-ik(x-y)]}{M_\phi^2 - k^2 - i\epsilon}. \end{aligned} \quad (28)$$

3 Electromagnetic form factors of the baryon octet

We define the electromagnetic form factors of the baryon in the Breit frame, where gauge invariance is fulfilled [3]. In this frame the initial momentum of the baryon is $p = (E, -\mathbf{q}/2 + \mathbf{\Delta})$, the final momentum is $p' = (E, \mathbf{q}/2 + \mathbf{\Delta})$, and the four-momentum of the photon is $q = (0, \mathbf{q})$ with $p' = p + q$. For identical baryons we have $\mathbf{\Delta} = 0$. With the space-like momentum transfer squared given as $Q^2 = -q^2 = \mathbf{q}^2$, we define the Sachs charge G_E^B and magnetic G_M^B form factors of the baryon as

$$\begin{aligned} \langle B'_{s'}(\frac{\mathbf{q}}{2} + \mathbf{\Delta}) | J^0(0) | B_s(-\frac{\mathbf{q}}{2} + \mathbf{\Delta}) \rangle \\ = \chi_{B'_{s'}}^\dagger \chi_{B_s} G_E^B(Q^2), \end{aligned} \quad (29)$$

$$\begin{aligned} \langle B'_{s'}(\frac{\mathbf{q}}{2} + \mathbf{\Delta}) | \mathbf{J}(0) | B_s(-\frac{\mathbf{q}}{2} + \mathbf{\Delta}) \rangle \\ = \chi_{B'_{s'}}^\dagger \frac{i\boldsymbol{\sigma}_B \times \mathbf{q}}{m_B + m_{B'}} \chi_{B_s} G_M^B(Q^2). \end{aligned} \quad (30)$$

Here, $J^0(0)$ and $\mathbf{J}(0)$ are the time and space components of the electromagnetic current operator; χ_{B_s} and $\chi_{B'_{s'}}^\dagger$ are the baryon spin WF in the initial and final states; $\boldsymbol{\sigma}_B$ is the baryon spin matrix. Electromagnetic gauge invariance both on the Lagrangian and the baryon level is fulfilled in the Breit frame [3].

At zero recoil ($q^2 = 0$) the Sachs form factors satisfy the following normalization conditions:

$$G_E^B(0) = Q_B, \quad G_M^B(0) = \mu_B, \quad (31)$$

where Q_B and μ_B are charge and magnetic moment of the baryon octet, respectively.

The charge and magnetic radii of baryons are given by

$$\langle r_{E,M}^2 \rangle^B = -\frac{6}{G_{E,M}^B(0)} \frac{d}{dQ^2} G_{E,M}^B(Q^2) \Big|_{Q^2=0}. \quad (32)$$

For neutral particles ($Q_B = 0$) the charge radius is defined by

$$\langle r_E^2 \rangle^B = -6 \frac{d}{dQ^2} G_E^B(Q^2) \Big|_{Q^2=0}. \quad (33)$$

In the PCQM the charge and magnetic form factors of the baryon octet are given as

$$\begin{aligned} &\chi_{s'}^\dagger \chi_s G_E^B(Q^2) \\ &= \langle \phi_0 | \sum_{n=0}^2 \frac{i^n}{n!} \int \delta(t) d^4x d^4x_1 \dots d^4x_n e^{-iq \cdot x} \\ &\times T[\mathcal{L}_r^{str}(x_1) \dots \mathcal{L}_r^{str}(x_n) j_r^0(x)] | \phi_0 \rangle^B, \end{aligned} \quad (34)$$

$$\begin{aligned} &\chi_{s'}^\dagger \frac{i\boldsymbol{\sigma}_B \times \mathbf{q}}{m_B + m_{B'}} \chi_s G_M^B(Q^2) \\ &= \langle \phi_0 | \sum_{n=0}^2 \frac{i^n}{n!} \int \delta(t) d^4x d^4x_1 \dots d^4x_n e^{-iq \cdot x} \\ &\times T[\mathcal{L}_r^{str}(x_1) \dots \mathcal{L}_r^{str}(x_n) \mathbf{j}_r(x)] | \phi_0 \rangle^B. \end{aligned} \quad (35)$$

The relevant diagrams contributing to the charge and magnetic form factors are indicated in Fig. 1. In the following we give the analytical expressions for the respective diagrams.

1. Three-quark diagram (3q):

$$G_{E,M}^B(Q^2) \Big|_{3q} = G_{E,M}^B(Q^2) \Big|_{3q}^{\text{LO}} + G_{E,M}^B(Q^2) \Big|_{3q}^{\text{NLO}}, \quad (36)$$

where $G_{E,M}^B(Q^2) \Big|_{3q}^{\text{LO}}$ are the leading-order (LO) terms of the three-quark diagram evaluated with the unperturbed quark WF $u_0(\mathbf{x})$; $G_{E,M}^B(Q^2) \Big|_{3q}^{\text{NLO}}$ is a correction due to the modification of the quark WF $u_0(\mathbf{x}) \rightarrow u_0^r(\mathbf{x}; m_i^r)$ referred to as next-to-leading order (NLO):

$$G_E^B(Q^2) \Big|_{3q}^{\text{LO}} = a_1^B G_E^p(Q^2) \Big|_{3q}^{\text{LO}}, \quad (37)$$

$$G_M^B(Q^2) \Big|_{3q}^{\text{LO}} = b_1^B \frac{m_B}{m_N} G_M^p(Q^2) \Big|_{3q}^{\text{LO}}, \quad (38)$$

$$G_E^B(Q^2) \Big|_{3q}^{\text{NLO}} = (a_2^B + a_3^B \varepsilon) G_E^p(Q^2) \Big|_{3q}^{\text{NLO}}, \quad (39)$$

$$G_M^B(Q^2) \Big|_{3q}^{\text{NLO}} = (b_2^B + b_3^B \varepsilon) \frac{m_B}{m_N} G_M^p(Q^2) \Big|_{3q}^{\text{NLO}}, \quad (40)$$

where

$$G_E^p(Q^2) \Big|_{3q}^{\text{LO}} = \exp\left(-\frac{Q^2 R^2}{4}\right) \left(1 - \frac{Q^2 R^2 \rho^2}{4(1 + \frac{3}{2}\rho^2)}\right), \quad (41)$$

$$G_E^p(Q^2) \Big|_{3q}^{\text{NLO}} = \exp\left(-\frac{Q^2 R^2}{4}\right) \hat{m}^r \frac{Q^2 R^3 \rho}{4(1 + \frac{3}{2}\rho^2)^2} \times \left(\frac{1 + 7\rho^2 + \frac{15}{4}\rho^4}{1 + \frac{3}{2}\rho^2} - \frac{Q^2 R^2}{4}\rho^2\right), \quad (42)$$

$$G_M^p(Q^2) \Big|_{3q}^{\text{LO}} = \exp\left(-\frac{Q^2 R^2}{4}\right) \frac{2m_N \rho R}{1 + \frac{3}{2}\rho^2}, \quad (43)$$

$$G_M^p(Q^2) \Big|_{3q}^{\text{NLO}} = G_M^p(Q^2) \Big|_{3q}^{\text{LO}} \frac{\hat{m}^r R \rho}{1 + \frac{3}{2}\rho^2} \times \left(\frac{Q^2 R^2}{4} - \frac{2 - \frac{3}{2}\rho^2}{1 + \frac{3}{2}\rho^2}\right), \quad (44)$$

and $\varepsilon = m_s^r/\hat{m}^r$. The constants a_i^B and b_i^B are given in Table 1 and Table 2, respectively. When using isospin symmetry we use for m_B , the baryon masses, following values

$$\begin{aligned} m_N &= m_p = m_n = 0.938 \text{ GeV}, \\ m_\Sigma &= m_{\Sigma^\pm} = m_{\Sigma^0} = 1.189 \text{ GeV}, \\ m_\Lambda &= 1.115 \text{ GeV}, \\ m_\Xi &= m_{\Xi^0} = m_{\Xi^-} = 1.321 \text{ GeV}, \\ m_{\Sigma^0\Lambda} &= \frac{1}{2}(m_\Sigma + m_\Lambda) = 1.152 \text{ GeV}. \end{aligned} \quad (45)$$

2. Three-quark counterterm (CT):

$$G_E^B(Q^2) \Big|_{\text{CT}} = [a_2^B(\hat{Z} - 1) + a_3^B(Z_s - 1)]G_E^p(Q^2) \Big|_{3q}^{\text{LO}}, \quad (46)$$

$$G_M^B(Q^2) \Big|_{\text{CT}} = [b_2^B(\hat{Z} - 1) + b_3^B(Z_s - 1)]\frac{m_B}{m_N}G_M^p(Q^2) \Big|_{3q}^{\text{LO}}. \quad (47)$$

3. Meson-cloud diagram (MC):

$$G_E^B(Q^2) \Big|_{\text{MC}} = \frac{9}{400} \left(\frac{g_A}{\pi F}\right)^2 \int_0^\infty dp p^2 \int_{-1}^1 dx \times \left(p^2 + p\sqrt{Q^2 x}\right) \mathcal{F}_{\pi NN}(p^2, Q^2, x) \times t_E^B(p^2, Q^2, x) \Big|_{\text{MC}}, \quad (48)$$

$$G_M^B(Q^2) \Big|_{\text{MC}} = \frac{3}{40} m_B \left(\frac{g_A}{\pi F}\right)^2 \int_0^\infty dp p^4 \int_{-1}^1 dx \times (1 - x^2) \mathcal{F}_{\pi NN}(p^2, Q^2, x) \times t_M^B(p^2, Q^2, x) \Big|_{\text{MC}}, \quad (49)$$

where

$$\mathcal{F}_{\pi NN}(p^2, Q^2, x) = F_{\pi NN}(p^2) F_{\pi NN}(p_+^2),$$

$$t_E^B(p^2, Q^2, x) \Big|_{\text{MC}} = a_4^B C_\pi^{11}(p^2, Q^2, x) + a_5^B C_K^{11}(p^2, Q^2, x),$$

$$t_M^B(p^2, Q^2, x) \Big|_{\text{MC}} = b_4^B D_\pi^{22}(p^2, Q^2, x) + b_5^B D_K^{22}(p^2, Q^2, x), \quad (50)$$

$$D_\Phi^{n_1 n_2}(p^2, Q^2, x) = \frac{1}{w_\Phi^{n_1}(p^2) w_\Phi^{n_2}(p_+^2)},$$

$$C_\Phi^{n_1 n_2}(p^2, Q^2, x) = \frac{2D_\Phi^{n_1 n_2}(p^2, Q^2, x)}{w_\Phi^{n_1}(p^2) + w_\Phi^{n_2}(p_+^2)},$$

$$p_\pm^2 = p^2 + Q^2 \pm 2p\sqrt{Q^2}.$$

4. Vertex-correction diagram (VC):

$$G_E^B(Q^2) \Big|_{\text{VC}} = G_E^p(Q^2) \Big|_{3q}^{\text{LO}} \frac{9}{200} \left(\frac{g_A}{\pi F}\right)^2 \times \int_0^\infty dp p^4 F_{\pi NN}^2(p^2) t_E^B(p^2) \Big|_{\text{VC}}, \quad (51)$$

$$G_M^B(Q^2) \Big|_{\text{VC}} = \frac{m_B}{m_N} G_M^p(Q^2) \Big|_{3q}^{\text{LO}} \frac{9}{200} \left(\frac{g_A}{\pi F}\right)^2 \times \int_0^\infty dp p^4 F_{\pi NN}^2(p^2) t_M^B(p^2) \Big|_{\text{VC}}, \quad (52)$$

where

$$\begin{aligned} t_E^B(p^2) \Big|_{\text{VC}} &= a_6^B W_\pi(p^2) + a_7^B W_K(p^2) \\ &\quad + a_8^B W_\eta(p^2), \\ t_M^B(p^2) \Big|_{\text{VC}} &= b_6^B W_\pi(p^2) + b_7^B W_K(p^2) \\ &\quad + b_8^B W_\eta(p^2), \\ W_\Phi(p^2) &= \frac{1}{w_\Phi^3(p^2)}. \end{aligned} \quad (53)$$

5. Meson-in-flight diagram (MF):

$$G_E^B(Q^2) \Big|_{\text{MF}} \equiv 0, \quad (54)$$

$$G_M^B(Q^2) \Big|_{\text{MF}} = \frac{9}{100} m_B \left(\frac{g_A}{\pi F}\right)^2 \int_0^\infty dp p^4 \times \int_{-1}^1 dx (1 - x^2) \mathcal{F}_{\pi NN}(p^2, Q^2, x) \times t_M^B(p^2, Q^2, x) \Big|_{\text{MF}}, \quad (55)$$

where

$$t_M^B(p^2, Q^2, x) \Big|_{\text{MF}} = b_9^B D_\pi^{22}(p^2, Q^2, x) + b_{10}^B D_K^{22}(p^2, Q^2, x). \quad (56)$$

Due to the use of a static potential the meson-in-flight diagram does not contribute to the charge baryon form factors.

The magnetic moments μ_B of the baryon octet are given by the expression (in units of the nucleon magneton μ_N)

$$\begin{aligned} \mu_B = \mu_B^{\text{LO}} & \left[1 + \delta (b_2^B + b_3^B \varepsilon) \right. \\ & - \frac{1}{400} \left(\frac{g_A}{\pi F} \right)^2 \int_0^\infty dp p^4 F_{\pi NN}(p^2) \\ & \times \left\{ \frac{k_1^B}{w_\pi^3} + \frac{k_2^B}{w_K^3} + \frac{k_3^B}{w_\eta^3} \right\} \\ & + \frac{m_B}{50} \left(\frac{g_A}{\pi F} \right)^2 \int_0^\infty dp p^4 F_{\pi NN}(p^2) \\ & \times \left\{ \frac{k_4^B}{w_\pi^4} + \frac{k_5^B}{w_K^4} \right\}, \end{aligned} \quad (57)$$

where

$$\mu_B^{\text{LO}} = b_1^B \frac{m_B}{m_N} G_M^p(0) \Big|_{3q}^{\text{LO}} = b_1^B \frac{2m_B \rho R}{1 + \frac{3}{2}\rho^2} \quad (58)$$

is the leading-order contribution to the baryon magnetic moment. The factor

$$\delta = -\hat{m}^r R \rho \frac{2 - \frac{3}{2}\rho^2}{(1 + \frac{3}{2}\rho^2)^2} \quad (59)$$

defines the NLO correction to the baryon magnetic moments due to the modification of the quark wave function (see Eq. (15)). The constants k_i^B are given in Table 3.

4 Numerical Results

Numerical results for the magnetic moments, charge and magnetic radii of the baryon octet are given in Tables 4, 5 and 6, respectively. The total results for the electromagnetic properties are separated into three parts: 1) the leading-order (3q[LO]) result due to the three quark core contribution; 2) the corrections (3q[NLO + CT]) to the three quark core contribution due to the renormalization of the quark WF (NLO) and the three-quark counterterm (CT) and 3) the effects of meson loops. The meson loop contributions include the meson-cloud (MC), the vertex-correction (VC), and the meson-in-flight (MF) diagrams. Experimental data are given in the last column of Tables. As was already mentioned, for a static potential the meson-in-flight diagram does not contribute to the baryon charge form factor. The range of our numerical results is due to variation of the size parameter R in the region 0.55

- 0.65 fm. The mesonic contributions to the baryon magnetic moments are of the order of 20 - 40 % (except for Ξ^- they contribute only 3 %). Hence, meson cloud corrections generate a significant influence on baryon magnetic moments. Our results for the baryon magnetic moments are in good agreement with the experimental data. Mesonic contributions to the charge radii of charged baryons are also of 20 - 40 % (except for Ξ^- where they contribute less than 1 %). We predict that

$$\langle r_E^2 \rangle^{\Sigma^+} > \langle r_E^2 \rangle^p > \langle r_E^2 \rangle^{\Sigma^-} > \langle r_E^2 \rangle^{\Xi^-}. \quad (60)$$

Our result for the proton and Σ^- charge radii squared are in good agreement with the experimental data. In the isospin limit the three-quark core does not contribute to the charge radii of neutral baryons. Only the meson cloud generates a nonvanishing value for the charge radii of these baryons. Since we restrict the quark propagator to the ground state contribution the meson-cloud effects give a small value for the neutron charge radius squared. We found that the result of the neutron charge radius can be improved by including excited states in the quark propagator. In Table 5 we give a comparison of our results for the neutron charge radius squared with the experimental value. The value, where the quark propagator is restricted to the ground state, is indicated by $\langle r_E^2 \rangle^n(\text{GS})$. Contributions from excited states (we have used $1p_{1/2}$, $1p_{3/2}$, $1d_{3/2}$, $1d_{5/2}$ and $2s_{1/2}$) are denoted by $\langle r_E^2 \rangle^n(\text{ES})$. Exemplified for the neutron charge radius, we conclude that excited state contributions can also generate sizable corrections when the LO results is vanishing. This result should be viewed as a first indication that excited quark state contributions are influential in ultimately determining observables which are dominated by loop diagrams. At this level a truncation following the $2s_{1/2}$ state is not necessarily justified by convergence arguments. An additional scale set by the finite size of the mesons should be introduced to restrict the contribution of intermediate excited quark states. In a further effort we intend to improve our calculations to the whole baryon octet by adding the excited states to the quark propagator and investigating its convergence properties. For Σ^0 , Λ and Ξ^0 we predict that their charge radii squared have a positive sign and follow the pattern

$$\langle r_E^2 \rangle^{\Xi^0} > \langle r_E^2 \rangle^{\Sigma^0} > \langle r_E^2 \rangle^\Lambda. \quad (61)$$

The mesons also play a very important role for the baryon magnetic radii where they contribute up to 50 %. Our result for the magnetic radius of Ξ^- is quite small compared to the other's because the meson-cloud contribution comes with a negative sign. Results for the magnetic radii squared of the proton and neutron are in good agreement with the experimental data.

The Q^2 -dependence (up to 0.4 GeV²) of the charge and magnetic form factors are shown in Figs. 2, 3, 4, 5 and 6. Due to the lack of covariance, the form factors can be expected to be reasonable up to $Q^2 < \mathbf{p}^2 = 0.4 \text{ GeV}^2$, where \mathbf{p} is the typical three-momentum transfer which

defines the region where relativistic effects $\leq 10\%$ or where the following inequality $\mathbf{p}^2/(4m_N^2) < 0.1$ is fulfilled. In Fig. 3 we compare our result for the neutron charge form factor to the experimental data varying the parameter R . Results are given for the case, where the quark propagator is restricted to the ground state. We separate the graphs for the charged and neutral baryons by using a proper normalization and compare to the experimental dipole fit, originally obtained for nucleon given by

$$G_D(Q^2) = \frac{1}{(1 + Q^2/0.71 \text{ GeV}^2)^2}. \quad (62)$$

There are also detailed analyses of the electromagnetic properties (magnetic moments, radii, form factors) of the baryon octet in literature. Because we are in the position to improve our formalism we relegate a detailed comparison to other theoretical approaches in our forthcoming paper. We just mention the recent papers [11,12] where a comprehensive analysis of baryon form factors (nucleons [11] and baryon octet [12]) was performed in the context of relativistic baryon chiral perturbation theory.

5 Summary

We apply the PCQM to calculate the charge and magnetic form factors of the baryon octet up to one loop perturbation theory. Furthermore, we analyze the magnetic moments, charge and magnetic radii. Since the PCQM is a static model, Lorentz covariance cannot be fulfilled. Approximate techniques to account for Galilei invariance and Lorentz boost effects were shown to change the tree level results by about 10 % [10]. Higher order, that is loop contributions, are less sensitive to these corrections. We demonstrated that meson cloud corrections play a sizable and important role in reproducing the experimental values both for magnetic moments and for the charge and magnetic radii. The magnetic moments of the baryon octet can be reproduced rather well. Also, charge and magnetic radii are explained with the PCQM, when the LO contribution, that is the valence quarks, dominates as soon as the LO result vanishes, meson cloud corrections which then control the observable tend to be sensitively influenced by the possible contributions of excited states in the loop diagrams. We demonstrated this effect for the case of the neutron charge radius, where inclusion of the excited states tend to improve the model result. Further investigations, which concern the role of excited states in calculating baryon observables are currently in progress.

In order to improve our model we are currently pursuing following aspects. First, we intend to improve our calculations to the whole baryon octet by adding the excited states to the quark propagator and investigating its convergence properties. Second, in order to improve the Q^2 -dependence of baryonic form factors we intend to include short-distance effects in addition to the light-meson cloud contributions which are important only at very low Q^2 . These short-distance effects might be taken into account by the use of low energy constants (LECs) as in

chiral perturbation theory or by the use of additional vector meson contributions as is well known to improve the intermediate Q^2 -dependence.

This work was supported by the DFG (Grant Nos. FA67/25-3, GRK 683). S.Cheedket and Y.Yan acknowledge the support of the DAAD (Grant No. a/00/27860) and Thailand Research Fund (TRF, Grant No. RGJ PHD/00165/2541). K.P. thanks the Development and Promotion of Science and Technology Talent Project (DPST), Thailand for financial support.

A Solutions of the Dirac equation for the effective potential

We state here again the variational Gaussian ansatz in Eq. (4)

$$u_0(\mathbf{x}) = N \exp\left[-\frac{\mathbf{x}^2}{2R^2}\right] \left(i\rho \boldsymbol{\sigma} \cdot \mathbf{x}/R\right) \chi_s \chi_f \chi_c, \quad (63)$$

This ansatz, when put back into the Dirac equation, restricts the form of the effective potential $V_{\text{eff}}(r)$ to be (note that $r = |\mathbf{x}|$)

$$V_{\text{eff}}(r) = S(r) + \gamma^0 V(r) \quad (64)$$

where the scalar $S(r)$ and time-like vector $V(r)$ parts are given by

$$\begin{aligned} S(r) &= M_1 + c_1 r^2, \\ V(r) &= M_2 + c_2 r^2, \end{aligned} \quad (65)$$

in which M_1 , M_2 , c_1 and c_2 are

$$\begin{aligned} M_1 &= \frac{1 - 3\rho^2}{2\rho R}, & M_2 &= \mathcal{E}_0 - \frac{1 + 3\rho^2}{2\rho R}, \\ c_1 &\equiv c_2 = \frac{\rho}{2R^3}. \end{aligned} \quad (66)$$

This specific choice of $V_{\text{eff}}(r)$ from the variational Gaussian ansatz will be used in obtaining the quark WF in any state. The quark WF $u_\alpha(\mathbf{x})$ in state α with eigenenergy \mathcal{E}_α satisfies the Dirac equation

$$[-i\boldsymbol{\alpha} \cdot \nabla + \beta S(r) + V(r) - \mathcal{E}_\alpha]u_\alpha(\mathbf{x}) = 0. \quad (67)$$

Due to our choice of the $V_{\text{eff}}(r)$ the Dirac equation can be solved analytically and the solutions of the Dirac spinor $u_\alpha(\mathbf{x})$ to Eq. (67) can be written in the form [21]

$$u_\alpha(\mathbf{x}) = N_\alpha \left(\begin{array}{c} g_\alpha(r) \\ i\boldsymbol{\sigma} \cdot \hat{\mathbf{x}} f_\alpha(r) \end{array} \right) \mathcal{Y}_\alpha(\hat{\mathbf{x}}) \chi_f \chi_c. \quad (68)$$

The radial functions $g_\alpha(r)$ and $f_\alpha(r)$ has the explicit form

$$g_\alpha(r) = \left(\frac{r}{R_\alpha}\right)^l L_{n-1}^{l+1/2}\left(\frac{r^2}{R_\alpha^2}\right) e^{-\frac{r^2}{2R_\alpha^2}}, \quad (69)$$

where for $j = l + \frac{1}{2}$

$$f_\alpha(r) = \rho_\alpha \left(\frac{r}{R_\alpha} \right)^{l+1} \left[L_{n-1}^{l+3/2} \left(\frac{r^2}{R_\alpha^2} \right) + L_{n-2}^{l+3/2} \left(\frac{r^2}{R_\alpha^2} \right) \right] e^{-\frac{r^2}{2R_\alpha^2}}, \quad (70)$$

and for $j = l - \frac{1}{2}$

$$f_\alpha(r) = -\rho_\alpha \left(\frac{r}{R_\alpha} \right)^{l-1} \left[\left(n + l - \frac{1}{2} \right) L_{n-1}^{l-1/2} \left(\frac{r^2}{R_\alpha^2} \right) + n L_n^{l-1/2} \left(\frac{r^2}{R_\alpha^2} \right) \right] e^{-\frac{r^2}{2R_\alpha^2}}. \quad (71)$$

The label $\alpha = (nljm)$ characterizes the state with principle quantum number $n = 1, 2, 3, \dots$, orbital angular momentum l , total angular momentum $j = l \pm \frac{1}{2}$ and projection m . Due to the quadratic nature of the potential the radial wave functions contain the associated Laguerre polynomials $L_n^k(x)$ with

$$L_n^k(x) = \sum_{m=0}^n (-1)^m \frac{(n+k)!}{(n-m)!(k+m)!m!} x^m. \quad (72)$$

The angular dependence $\mathcal{Y}_\alpha(\hat{\mathbf{x}}) \equiv \mathcal{Y}_{lmj}(\hat{\mathbf{x}})$ is defined by

$$\mathcal{Y}_{lmj}(\hat{\mathbf{x}}) = \sum_{m_l, m_s} (lm_l \frac{1}{2} m_s | jm) Y_{lm_l}(\hat{\mathbf{x}}) \chi_{\frac{1}{2} m_s} \quad (73)$$

where $Y_{lm_l}(\hat{\mathbf{x}})$ is the usual spherical harmonic. χ_f and χ_c are the flavor and color part of the Dirac spinor, respectively.

The coefficients R_α and ρ_α which belong to the α state are of the form

$$R_\alpha = R(1 + \Delta\mathcal{E}_\alpha \rho R)^{-1/4}, \quad (74)$$

$$\rho_\alpha = \rho \left(\frac{R_\alpha}{R} \right)^3$$

and are related to the Gaussian parameters ρ , R of Eq. (63). Here we define $\Delta\mathcal{E}_\alpha = \mathcal{E}_\alpha - \mathcal{E}_0$ to be the difference between the energy of state α and the ground state. $\Delta\mathcal{E}_\alpha$ depends on the quantum numbers n and l and is related to the parameters ρ and R by

$$(\Delta\mathcal{E}_\alpha + \frac{3\rho}{R})^2 (\Delta\mathcal{E}_\alpha + \frac{1}{\rho R}) = \frac{\rho}{R^3} (4n + 2l - 1)^2. \quad (75)$$

The normalization condition is

$$\int_0^\infty d^3x u_\alpha^\dagger(\mathbf{x}) u_\alpha(\mathbf{x}) = 1 \quad (76)$$

with this condition the normalization constant N_α is of the form

$$N_\alpha = \left[2^{-2(n+l+1/2)} \pi^{1/2} R_\alpha^3 \frac{(2n+2l)!}{(n+l)!(n-1)!} \times \left\{ 1 + \rho_\alpha^2 (2n+l - \frac{1}{2}) \right\} \right]^{-1/2}. \quad (77)$$

References

1. I. Eschrich *et al.* [SELEX Collaboration], Phys. Lett. B **522**, (2001) 233.
2. M. I. Adamovich *et al.* [WA89 Collaboration], Eur. Phys. J. C **8**, (1999) 59.
3. V. E. Lyubovitskij, Th. Gutsche and A. Faessler, Phys. Rev. C **64**, (2001) 065203.
4. V. E. Lyubovitskij, Th. Gutsche, A. Faessler and E.G. Drukarev, Phys. Rev. D **63**, (2001) 054026.
5. V. E. Lyubovitskij, Th. Gutsche, A. Faessler and R. Vinh Mau, Phys. Lett. B **520**, (2001) 204; Phys. Rev. C **65**, (2002) 025202.
6. V. E. Lyubovitskij, P. Wang, Th. Gutsche and A. Faessler, Phys. Rev. C **66**, (2002) 055204.
7. F. Simkovic, V.E. Lyubovitskij, Th. Gutsche, A. Faessler and S. Kovalenko, Phys. Lett. B **544**, (2002) 121.
8. K. Pumsa-ard, V. E. Lyubovitskij, Th. Gutsche, A. Faessler and S. Cheedket, Phys. Rev. C **68**, (2003) 015205.
9. M. C. Birse, Prog. Part. Nucl. Phys. **25**, (1990) 1.
10. D. H. Lu, A. W. Thomas and A. G. Williams, Phys. Rev. C **57**, (1998) 2628.
11. B. Kubis and U.-G. Meißner, Nucl. Phys. A **679**, (2001) 698.
12. B. Kubis and U.-G. Meißner, Eur. Phys. J. C **18**, (2001) 747.
13. K. Hagiwara *et al.* [Particle Data Group Collaboration], Phys. Rev. D **66**, (2002) 010001.
14. G. G. Simon, F. Borkowski, C. Schmitt and V. H. Walther, Z. Naturforsch. **35A**, (1980) 1.
15. G. Kubon *et al.*, Phys. Lett. B **524**, (2002) 26.
16. M. Ostrick *et al.*, Phys. Rev. Lett. **83**, (1999) 276.
17. J. Becker *et al.*, Eur. Phys. J. A **6**, (1999) 329.
18. M. Meyerhoff *et al.*, Phys. Lett. B **327**, (1994) 201.
19. C. Herberg *et al.*, Eur. Phys. J. A **5**, (1999) 131.
20. T. Eden *et al.*, Phys. Rev. C **50**, (1994) R1749.
21. R. Tegen, R. Brockmann and W. Weise, Z. Phys. A **307**, (1982) 339.

Table 1. The constants a_i^B for the charge form factors G_E^B of the baryon octet.

	p	n	Σ^+	Σ^0	Σ^-	Λ	Ξ^0	Ξ^-	$\Sigma^0 \Lambda$
a_1	1	0	1	0	-1	0	0	-1	0
a_2	1	0	$\frac{4}{3}$	$\frac{1}{3}$	$-\frac{2}{3}$	$\frac{1}{3}$	$\frac{2}{3}$	$-\frac{1}{3}$	0
a_3	0	0	$-\frac{1}{3}$	$-\frac{1}{3}$	$-\frac{1}{3}$	$-\frac{1}{3}$	$-\frac{2}{3}$	$-\frac{2}{3}$	0
a_4	1	-1	2	0	-2	0	1	-1	0
a_5	2	1	1	0	-1	0	-1	-2	0
a_6	$\frac{1}{2}$	1	0	$\frac{1}{2}$	1	$\frac{1}{2}$	0	$\frac{1}{2}$	0
a_7	-1	-1	$-\frac{1}{3}$	$-\frac{1}{3}$	$-\frac{1}{3}$	$-\frac{1}{3}$	$\frac{1}{3}$	$\frac{1}{3}$	0
a_8	$\frac{1}{6}$	0	0	$-\frac{1}{6}$	$-\frac{1}{3}$	$-\frac{1}{6}$	$-\frac{1}{3}$	$-\frac{1}{2}$	0

Table 2. The constants b_i^B for the magnetic form factors G_M^B of the baryon octet.

	p	n	Σ^+	Σ^0	Σ^-	Λ	Ξ^0	Ξ^-	$\Sigma^0 \Lambda$
b_1	1	$-\frac{2}{3}$	1	$\frac{1}{3}$	$-\frac{1}{3}$	$-\frac{1}{3}$	$-\frac{2}{3}$	$-\frac{1}{3}$	$-\frac{\sqrt{3}}{3}$
b_2	1	$-\frac{2}{3}$	$\frac{8}{9}$	$\frac{2}{9}$	$-\frac{4}{9}$	0	$-\frac{2}{9}$	$\frac{1}{9}$	$-\frac{\sqrt{3}}{3}$
b_3	0	0	$\frac{1}{9}$	$\frac{1}{9}$	$\frac{1}{9}$	$-\frac{1}{3}$	$-\frac{4}{9}$	$-\frac{4}{9}$	0
b_4	1	-1	$\frac{4}{5}$	0	$-\frac{4}{5}$	0	$-\frac{1}{5}$	$\frac{1}{5}$	$-\frac{2\sqrt{3}}{5}$
b_5	$\frac{4}{5}$	$-\frac{1}{5}$	1	$\frac{3}{5}$	$\frac{1}{5}$	$-\frac{3}{5}$	-1	$-\frac{4}{5}$	$-\frac{\sqrt{3}}{5}$
b_6	$\frac{1}{18}$	$-\frac{2}{9}$	0	$-\frac{1}{9}$	$-\frac{2}{9}$	0	0	$\frac{1}{18}$	$-\frac{\sqrt{3}}{18}$
b_7	$\frac{1}{9}$	$\frac{1}{9}$	$\frac{5}{27}$	$\frac{5}{27}$	$\frac{5}{27}$	$-\frac{1}{9}$	$-\frac{5}{27}$	$-\frac{5}{27}$	0
b_8	$-\frac{1}{18}$	$\frac{1}{27}$	$-\frac{2}{27}$	$-\frac{1}{27}$	0	$\frac{2}{27}$	$\frac{1}{9}$	$\frac{5}{54}$	$\frac{\sqrt{3}}{54}$
b_9	1	-1	0	0	0	0	0	0	$-\frac{\sqrt{3}}{3}$
b_{10}	0	0	1	1	1	-1	-1	-1	0

Table 3. The constants k_i^B for the magnetic moment μ_B of the baryon octet.

	p	n	Σ^+	Σ^0	Σ^-	Λ	Ξ^0	Ξ^-	$\Sigma^0 \Lambda$
k_1	26	21	24	24	24	30	9	-6	24
k_2	16	21	$\frac{50}{3}$	14	22	0	25	32	18
k_3	4	4	$\frac{16}{3}$	8	0	16	12	20	4
k_4	11	-11	4	3	-4	-3	-1	1	$-4\sqrt{3}$
k_5	4	-1	11	6	7	-6	-11	-10	$-\sqrt{3}$

Table 4. Results for the magnetic moments μ_B of the baryon octet (in units of the nucleon magneton μ_N).

	3q [LO]	3q [NLO+CT]	Meson loops [MC+VC+MF]	Total	Exp [13]
μ_p	1.80 ± 0.15	0.01 ± 0.03	0.79 ± 0.12	2.60 ± 0.03	2.793
μ_n	-1.20 ± 0.10	-0.01 ± 0.02	-0.77 ± 0.12	-1.98 ± 0.02	-1.913
μ_{Σ^+}	2.28 ± 0.19	-0.04 ± 0.04	0.51 ± 0.11	2.75 ± 0.09	2.458 ± 0.010
μ_{Σ^0}	0.76 ± 0.06	-0.05 ± 0.02	0.34 ± 0.07	1.05 ± 0.01	—
μ_{Σ^-}	-0.76 ± 0.06	-0.06 ± 0.01	-0.26 ± 0.02	-1.08 ± 0.05	-1.160 ± 0.025
μ_Λ	-0.71 ± 0.06	0.15 ± 0.04	-0.33 ± 0.09	-0.89 ± 0.03	-0.613 ± 0.004
μ_{Ξ^0}	-1.69 ± 0.14	0.23 ± 0.09	-0.28 ± 0.11	-1.74 ± 0.03	-1.250 ± 0.014
μ_{Ξ^-}	-0.85 ± 0.07	0.23 ± 0.06	-0.05 ± 0.07	-0.68 ± 0.01	-0.651 ± 0.003
$ \mu_{\Sigma^0\Lambda} $	1.28 ± 0.11	0.01 ± 0.02	0.61 ± 0.09	1.89 ± 0.01	1.61 ± 0.08

Table 5. Results for the charge radii squared $\langle r_E^2 \rangle^B$ of the baryon octet (in units of fm²).

	3q [LO]	3q [NLO+CT]	Meson loops [MC+VC]	Total	Exp
$\langle r_E^2 \rangle^p$	0.60 ± 0.10	0.004 ± 0.004	0.12 ± 0.01	0.72 ± 0.09	0.76 ± 0.02 [13]
$\langle r_E^2 \rangle_{\text{GS}}^n$	0	0	-0.043 ± 0.004	-0.043 ± 0.004	
$\langle r_E^2 \rangle_{\text{ES}}^n$	0	0	-0.068 ± 0.013	-0.068 ± 0.013	
$\langle r_E^2 \rangle_{\text{Full}}^n$	0	0	-0.111 ± 0.014	-0.111 ± 0.014	-0.116 ± 0.002 [13]
$\langle r_E^2 \rangle^{\Sigma^+}$	0.60 ± 0.10	0.07 ± 0.004	0.14 ± 0.004	0.81 ± 0.10	—
$\langle r_E^2 \rangle^{\Sigma^0}$	0	0.038 ± 0.010	0.012 ± 0.010	0.050 ± 0.010	—
$\langle r_E^2 \rangle^{\Sigma^-}$	0.60 ± 0.10	-0.04 ± 0.01	0.15 ± 0.03	0.71 ± 0.07	0.61 ± 0.21 [1]
$\langle r_E^2 \rangle^\Lambda$	0	0.038 ± 0.010	0.012 ± 0.010	0.050 ± 0.010	—
$\langle r_E^2 \rangle^{\Xi^0}$	0	0.07 ± 0.02	0.07 ± 0.02	0.14 ± 0.02	—
$\langle r_E^2 \rangle^{\Xi^-}$	0.60 ± 0.10	-0.08 ± 0.03	0.10 ± 0.03	0.62 ± 0.07	—
$\langle r_E^2 \rangle^{\Sigma^0\Lambda}$	0	0	0	0	—

Table 6. Results for the magnetic radii squared $\langle r_M^2 \rangle^B$ of the baryon octet (in units of fm²).

	3q [LO]	3q [NLO+CT]	Meson loops [MC+VC+MF]	Total	Exp
$\langle r_M^2 \rangle^p$	0.37±0.09	0.03±0.001	0.34±0.02	0.74± 0.07	0.74±0.10 [14]
$\langle r_M^2 \rangle^n$	0.33±0.08	0.03±0.002	0.43±0.01	0.79± 0.07	0.76±0.02 [15]
$\langle r_M^2 \rangle^{\Sigma^+}$	0.45±0.10	0.02±0.006	0.17±0.02	0.64± 0.08	—
$\langle r_M^2 \rangle^{\Sigma^0}$	0.39±0.10	-0.02±0.01	0.32±0.03	0.69± 0.07	—
$\langle r_M^2 \rangle^{\Sigma^-}$	0.38±0.08	0.09±0.01	0.31±0.01	0.78± 0.07	—
$\langle r_M^2 \rangle^\Lambda$	0.44±0.12	-0.14±0.06	0.35±0.07	0.65± 0.05	—
$\langle r_M^2 \rangle^{\Xi^0}$	0.52±0.12	-0.01±0.04	0.03±0.05	0.54± 0.06	—
$\langle r_M^2 \rangle^{\Xi^-}$	0.67±0.17	-0.31±0.12	-0.04±0.13	0.32± 0.04	—
$\langle r_M^2 \rangle^{\Sigma^0 \Lambda}$	0.36±0.09	0.03±0.001	0.36±0.02	0.75± 0.07	—

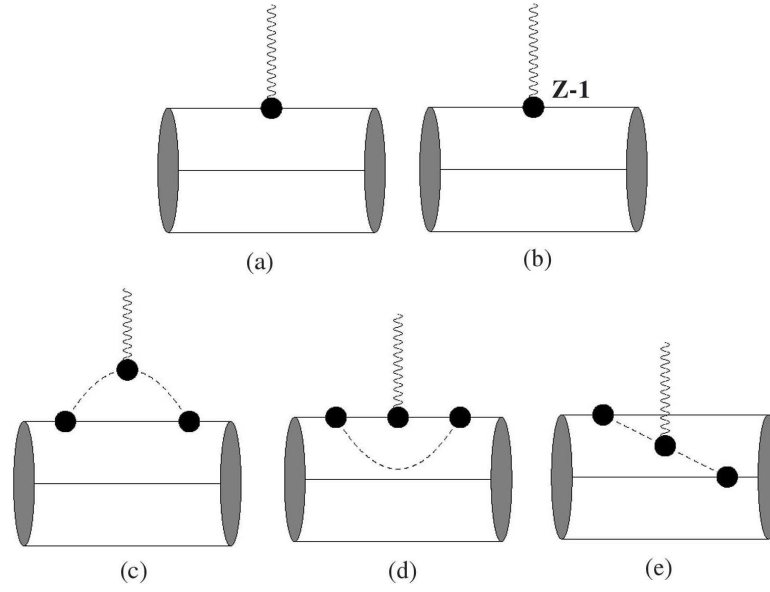


Fig. 1. Diagrams contributing to the charge and magnetic form factors of the baryon octet: three-quark diagram (a), three-quark counterterm diagram (b), meson-cloud diagram (c), vertex correction diagram (d), and meson-in-flight diagram (e).

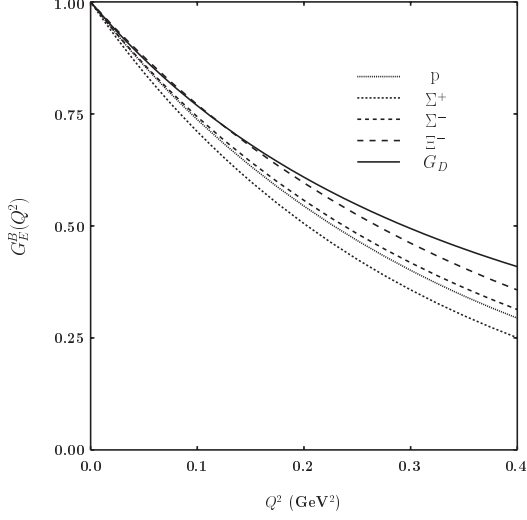


Fig. 2. The charge form factors $G_E^B(Q^2)$ for $B = p, \Sigma^+, \Sigma^-$ and Ξ^- for $R = 0.6$ fm compared to the dipole fit $G_D(Q^2)$. For Σ^- and Ξ^- , the absolute value of $G_E^B(Q^2)$ is shown.

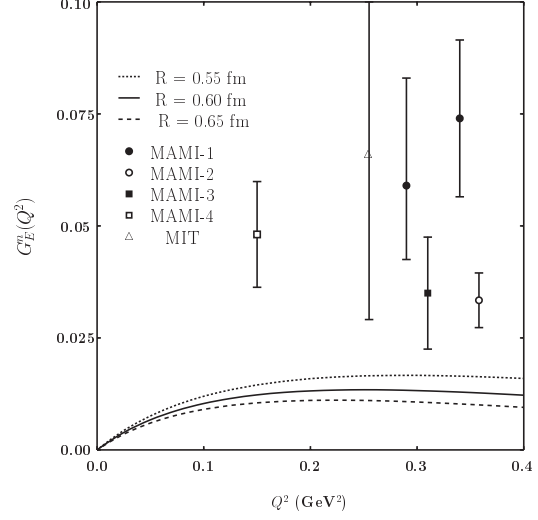


Fig. 3. The neutron charge form factors $G_E^n(Q^2)$ for different values of $R = 0.55, 0.6$, and 0.65 fm. Experimental data are taken from [16](MAMI-1), [17](MAMI-2), [18](MAMI-3), [19](MAMI-4), and [20](MIT).

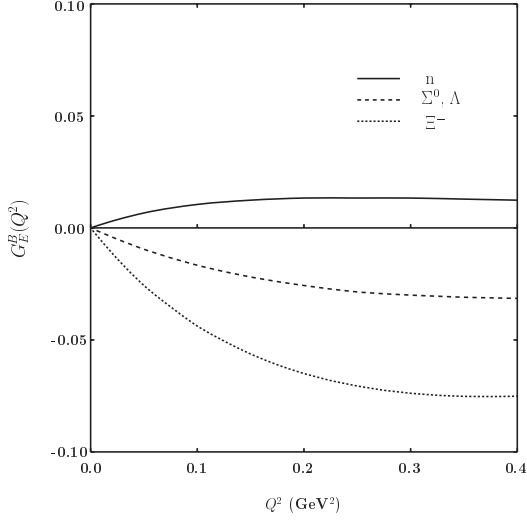


Fig. 4. The charge form factors $G_E^B(Q^2)$ for $B = n, \Sigma^0, \Lambda$ and Ξ^- at $R = 0.6$ fm.

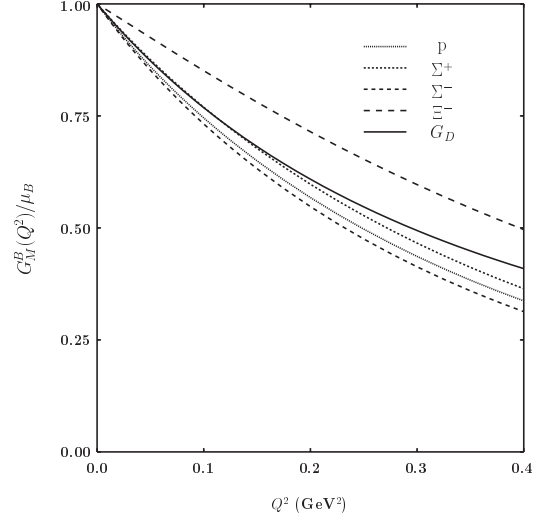


Fig. 5. The normalized magnetic form factors $G_M^B(Q^2)/\mu_B$ for $B = p, \Sigma^+, \Sigma^-$ and Ξ^- at $R = 0.6$ fm in comparison to the dipole fit $G_D(Q^2)$.

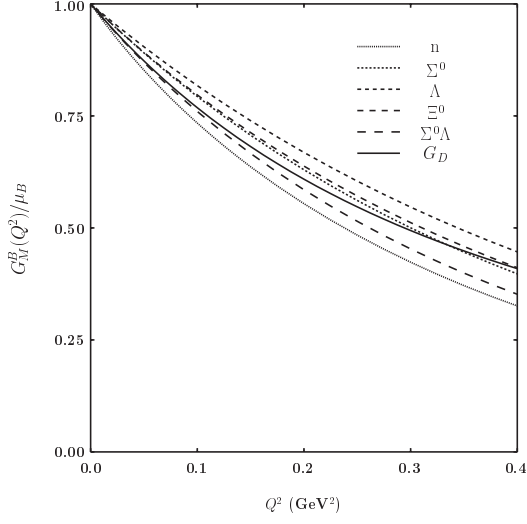


Fig. 6. The normalized magnetic form factors $G_M^B(Q^2)/\mu_B$ for $B = n, \Sigma^0, \Lambda$ and Ξ^0 at $R = 0.6$ fm as compared to the dipole fit $G_D(Q^2)$.